International Journal of Nanoelectronics and Materials
IJNeaM
ISSN 1985-5761 | E-ISSN 2232-1535

Removal of methylene blue using trifunctional magnetic polyethersulfone microcapsule: Process parameters and optimization study

Suh Cia Yong [a] *, Siew Hoong Shuit [a,b,*], Wei Yang Tan [a], Qi Hwa Ng [c,d], Steven Lim [a,b], Hui San Thiam [a,b], Shiau Foon Tee [a], Kok Chung Chong [a,b], and Peng Yong Hoo [c,d]

[a] *Department of Chemical Engineering, Lee Kong Chian Faculty of Engineering and Science (LKCFES), Universiti Tunku Abdul Rahman (UTAR), Sungai Long Campus, Jalan Sungai Long, Bandar Sungai Long, Cheras, 43000, Kajang, Selangor, Malaysia*
[b] *Centre for Advanced and Sustainable Materials Research (CASMR), Sungai Long Campus, Universiti Tunku Abdul Rahman (UTAR), Jalan Sungai Long, Bandar Sungai Long, Cheras, Kajang 43000, Selangor, Malaysia*
[c] *Faculty of Chemical Engineering & Technology, Universiti Malaysia Perlis (UniMAP), Perlis, Malaysia*
[d] *Centre of Excellence for Frontier Materials Research (CFMR), Universiti Malaysia Perlis (UniMAP), Perlis, Malaysia*
∗ *Corresponding author. Tel.: +6-016-541-6632; e-mail: shuitsh@utar.edu.my*

Received 28 April 2024, Revised 7 August 2024, Accepted 25 August 2024

ABSTRACT

Water pollution from dye-contaminated effluents poses a critical environmental threat. Current dye removal methods often rely on activated carbon, which is expensive and challenging to recover. This study focuses on the removal of methylene blue (MB), a cationic dye, using trifunctional polyethersulfone (PES)-encapsulated polydimethyldiallyl ammonium chloride-functionalized iron oxide (PDDA-Fe_3O_4) microcapsules with adsorptive, catalytic, and magnetic properties. The negatively charged PES facilitates MB adsorption through electrostatic interactions, while Fe_3O_4 enhances Fenton degradation and imparts magnetic responsiveness. Characterization techniques, including Fourier transform infrared spectroscopy and scanning electron microscopy with energy-dispersive X-ray analysis, confirmed the presence of PDDA-coated Fe_3O_4 and the formation of porous structures and finger-like cavities in the microcapsules. Process parameters such as microcapsule loading (10-30 g/L), MB concentration (10-50 ppm), pH (2-10), contact time (60-240 min), and H_2O_2 concentration (0.1-1 mol/L) were optimized using response surface methodology with a central composite design. Optimal conditions for MB removal (92.94%) were achieved with 21 g/L of microcapsules, 25 ppm of MB, pH 7, 127 minutes of contact time, and 0.45 mol/L of H_2O_2. These results demonstrate the efficacy of PDDA-Fe_3O_4@PES microcapsules for dye removal and suggest their potential for application in industries such as textiles and cosmetics, which generate high volumes of dye-contaminated wastewater.

Keywords: *Magnetic microcapsule, Fenton-like degradation, Adsorption, Methylene blue, Optimization*

1. INTRODUCTION

Industrial usage of synthetic dyes has significantly risen over the last few decades, especially in dyestuff, cosmetics, paper, plastics, leather, and textile industries, making it one of the main sources of cationic pollutants. Among various industries, the most often used cationic dye for coloring is methylene blue (MB). Besides being used as dye, MB is also applied in the medical sector as a staining agent and in treating cyanide poisoning and methemoglobinemia. Despite its wide application, MB has a lot of harmful effects on living things, including irritation on various body part, causes diarrhea, vomiting, redness, and itching [1]. MB pollution can also be critical for aquatic biosystems since cationic pollutants can reduce sunlight transmission. The contaminant-induced inhibition of the photosynthetic activity will bring serious negative impact to the symbiotic processes of aquatic ecosystem [2]. Thus, from both a human and environmental perspective, the removal of MB dye from wastewater is of major concern nowadays.

Various techniques were employed for the removal of cationic pollutants from effluents. Among all available techniques, adsorption is one of the most superior approaches that has been widely implanted due to its construction and operational simplicity, low energy consumption, and is more effective in removing various harmful contaminants. However, recovery of activated carbon (AC) from the liquid phase was a challenging process. This is due to the difficulty of separating AC from water bodies and the separation process often produce secondary pollutants, specifically dust pollution [3]. In addition, waste dye generated during the adsorbent's regeneration process using solvent extraction also contributed to the secondary pollution [4]. Moreover, AC also has rather high capital cost. This issue is brought on by the expensive synthesis of AC and the complicated synthesis procedures.

Hence, in this study, a trifunctional polyethersulfone encapsulated polydimethyldiallyl ammonium chloride functionalized iron oxide (PDDA-Fe_3O_4@PES) microcapsule which exhibits outstanding magnetic responsive, catalytic and adsorptive properties, making it highly effective for removing cationic water pollutants, was synthesized. The microcapsule consists of a magnetic-responsive polymer

nanocomposite, with polydimethyldiallyl ammonium chloride (PDDA) functionalized iron oxide (Fe_3O_4) as the inner core and a negatively charged polyether sulfone (PES) shell. Beyond its magnetic responsiveness, Fe_3O_4 nanoparticles act as catalysts in the Fenton-like degradation process, a cost-effective oxidation method for dye removal. With the presence of hydrogen peroxide (H_2O_2) [5], Fe_3O_4 nanoparticles facilitate the production of hydroxyl radicals (•OH) that can break down MB contaminants into water and carbon dioxide [6]. Additionally, the negative surface charge of the PES shell makes the microcapsule an excellent adsorbent for cationic MB, through electrostatic attraction between oppositely charged particles [7]. Therefore, the novelty of the PDDA-Fe_3O_4@PES microcapsule lies in its ability to remove dye pollutants through simultaneous adsorption and degradation.

The trifunctional microcapsule is designed to address the limitations of AC. AC used in adsorption processes requires additional steps to remove the spent AC from treated water, such as membrane filtration, coagulation/flocculation, or centrifugation, which increases energy consumption, complexity, and operational costs. In contrast, the synthesized PDDA-Fe_3O_4@PES microcapsule, with its superior magnetic responsiveness, can be easily recovered using an external magnetic field. Moreover, a major disadvantage of AC is the regeneration and recycling process, which generates secondary waste. The PDDA-Fe_3O_4@PES microcapsule, capable of initiating the Fenton-like degradation process, can be reused without regeneration while maintaining high pollutant removal efficiency. Thus, this study aimed to investigate and optimize various process parameters, such as microcapsule loading, initial MB concentration, pH, contact time and H_2O_2 concentration for the removal of MB using PDDA-Fe_3O_4@PES microcapsule.

2. MATERIALS AND METHODS

2.1. Materials

Polydimethyldiallyl ammonium chloride (35 wt% in H_2O), Iron (III) chloride hexahydrate ($FeCl_3 \cdot 6H_2O$), Iron (II) chloride tetrahydrate ($FeCl_2 \cdot 4H_2O$), hydrochloric acid (HCL) and sodium hydroxide (NaOH) were purchased from Sigma-Aldrich, Malaysia while ammonia solution (NH_4OH, 30 wt% in H_2O) were supplied by R&M Chemical, Malaysia. Polyethersulfone granule (purity >99%) was purchased from BASF, Malaysia, N-methyl-2-pyrrolidone (NMP, purity >99.9%) from Merck, Malaysia and Polyethylene Glycol (PEG, purity >99.5%) from Chemicals Solutions Sdn. Bhd., Malaysia. All the chemicals were of analytical grade and used as received without undergoing further purification procedures.

2.2. Synthesis of PDDA Functionalized Fe_3O_4 NPs

The PDDA-Fe_3O_4 nano particles (NPs) were synthesized as described in [8]. A beaker was filled with 2.16 g of $FeCl_3 \cdot 6H_2O$ and 0.8 g of $FeCl_2 \cdot 4H_2O$. Next, 20 mL of deionized water was added to the beaker, after which 0.6 g (1 v.t. %) of PDDA was introduced, and the mixture was then heated to 80 °C. To precipitate PDDA-Fe_3O_4 NPs, 10 mL of NH_4OH solution was then added to the heated mixture. At 200 rpm, the mixture was stirred for an hour. Upon completion, the mixture underwent ultrasonication (35 kHz, 200W) for 30 minutes to aid in the dissolution of the PDDA-Fe_3O_4 NPs. The mixture was then quickly cooled to room temperature. Finally, a permanent magnet was used to harvest the PDDA-Fe_3O_4 NPs. The NPs were air dried after being thoroughly cleaned with deionized water.

2.3. Synthesis of PDDA-Fe_3O_4@PES Microcapsule

The PDDA-Fe_3O_4@PES microcapsule was synthesized as described in [8]. 2 g (10 wt %) of PES flakes and 1 g (5 wt. %) of PEG flakes were dissolved in 18 g of NMP solvent to produce the prepolymer solution for the encapsulation process. PES functioned as a component of the microcapsule's shell wall, and PEG acted as a pore-forming agent. The mixture was stirred at 180 rpm for 60 minutes while being maintained at a temperature of 70°C. After that, the mixture was cool to ambient temperature while being constantly stirred to maintain the solution's homogeneity. Phase inversion method was used to synthesis the PDDA-Fe_3O_4 @PES microcapsule. 0.4 g (2 wt. %) of PDDA-Fe_3O_4 NPs were mixed with 20 mL of prepolymer solution. The mixture was sonicated (35 kHz, 200 W) for 30 minutes. The mixture was injected into the distilled water using a syringe needle with a diameter of 0.46 mm (size 26G) at a 0.1 mL/min rate with the help of peristaltic pump.

The prepolymer solution was added into the deionized water in dropwise manner and phase inversion resulted in the precipitation of PDDA-Fe_3O_4@PES microcapsule. Throughput the phase inversion process, the microcapsule-forming solution was agitated to prevent settling of NPs. The magnetic microcapsules were isolated from the solution using a magnet, rinsed thoroughly with deionized water, and subsequently immersed in deionized water overnight. Finally, the microcapsule was air-dried at room temperature.

2.4. Characterization of PDDA-Fe_3O_4@PES Microcapsule

Scanning electron microscopy coupled with energy-dispersive X-ray (SEM-EDX, Hitachi S-3400N scanning electron microscopy) at 15.0 kV accelerating voltage was used to examine the surface morphology and the elemental composition of the PDDA-Fe_3O_4@PES microcapsule. Fourier transform infrared spectroscopy (FTIR, Nicolet IS10) via attenuated total reflection (ATR) method was used to identify the functional groups on the produced microcapsule. 32 cumulative scans at a wavenumber of 4000 to 400 cm^{-1} were used for the FTIR analysis.

2.5. Removal of MB Using PDDA-Fe_3O_4@PES Microcapsule

A conical flask was filled with a total volume of 30 mL solution containing MB, H_2O_2 and distilled water. Then, a predetermined quantity of PDDA-Fe_3O_4@PES microcapsule was added into the solution. Next, the removal process was

performed in a shaker for a predetermined amount of time. Upon completion, the microcapsule was removed from the solution using a permanent magnet. The concentration of the MB solution was determined using a UV-Vis spectrophotometer at a wavelength of 664 nm. The efficiency of dye removal was calculated using Equation 1.

$$Efficiency\ (\%) = \frac{C_i - C_f}{C_i} \times 100 \quad (1)$$

Where C_i and C_f are the initial and final concentration (mg/L) of MB dye in the solution, respectively.

2.6. Statistical Analysis and Optimization Using Design of Experiments (DOE)

The design of experiments selected for the process study and optimization process was respond surface methodology (RSM) coupled with central composite design (CCD) using the Design Expert 12 software. A total of 50 runs (including 8 repeated runs at the central point) were generated to examine the five independent variables at five levels (-α, -1, 0, +1, +α) as shown in Table 1. The parameters for each set of experiments include microcapsule loading, MB concentration, solution pH, H_2O_2 concentration and contact time. The response of this design was the removal of MB (%). Each experiment run was carried out in triplicate and average results were recorded.

Table 1. Range of parameters for optimization study

Factor	Code	Unit	Levels				
			-α	-1	0	+1	+α
Microcapsule loading	A	g/L	10	16	20	24	30
Initial MB concentration	B	mg/L	10	22	30	38	50
Solution pH	C	-	2	4	6	8	10
Contact time	D	min	60	112	120	188	240
H_2O_2 concentration	E	mol/L	0.10	0.36	0.55	0.74	1.00

3. RESULTS AND DISCUSSION

3.1. Characterization Results of PDDA-Fe_3O_4@PES Microcapsule

Figure 1 (a) and (b) display the surface morphology and the cross-sectional view of the PDDA-Fe_3O_4@PES microcapsule, respectively.

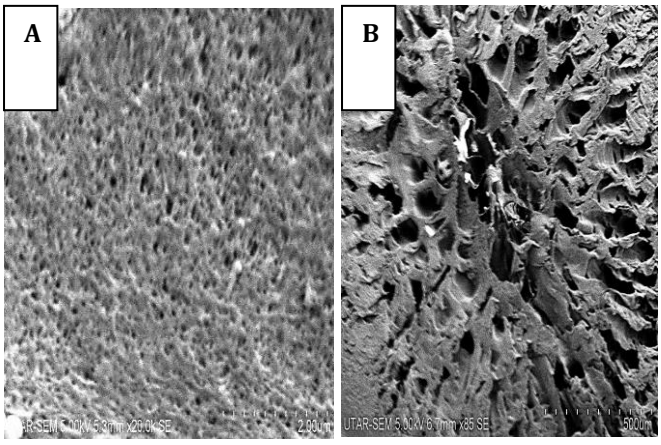

Figure 1. SEM images of (a) PDDA-Fe_3O_4@PES microcapsule 5.3 mm x 20.0k SE of magnification, (b) cross-sectional view of the microcapsule 6.7 mm x 85 SE of magnification.

Figure 1 (a) depicts the scattering distribution of pores developed on the surface of PDDA-Fe_3O_4@PES microcapsule Besides, through the cross-sectional view of the microcapsule as shown in Figure 2 (b), the porous finger-like structure was clearly visible. This occurrence was attributed to the interchange occurring between the solvent and non-solvent across the boundary layer during the phase inversion before the PES polymer fully solidified. The use of ultrasonication after the phase inversion process may have contributed to the very porous structure of the PDDA-Fe_3O_4@PES microcapsule. According to [9], the significant shearing impact of powerful ultrasound can disturb the surface of microcapsule and cause the development of additional pores. On top of that, the additional of PEG polymer and PDDA-Fe_3O_4 NPs can alter the chemical compositions and physical features of the microcapsule forming solution. As a results, pores were developed in the PDDA-Fe_3O_4@PES microcapsule in all directions [10].

The EDX result of the PDDA-Fe_3O_4@PES microcapsule is shown in Figure 2. In PDDA-Fe_3O_4@PES microcapsule, the weight percentages of iron (Fe) and oxygen (O) were discovered to be 2.23 % and 22.08 %, respectively. The EDX results demonstrated that PDDA-Fe_3O_4 NPs were successfully encapsulated into the microcapsule.

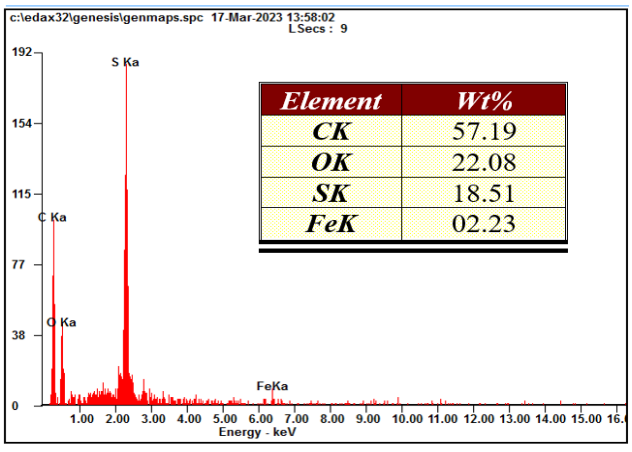

Figure 2. EDX results of PDDA-Fe_3O_4@PES microcapsule

The FTIR spectra of the naked Fe_3O_4, PDDA-Fe_3O_4 NPs and PDDA-Fe_3O_4@PES microcapsule are shown in Figure 3, Figure 4, and Figure 5, respectively.

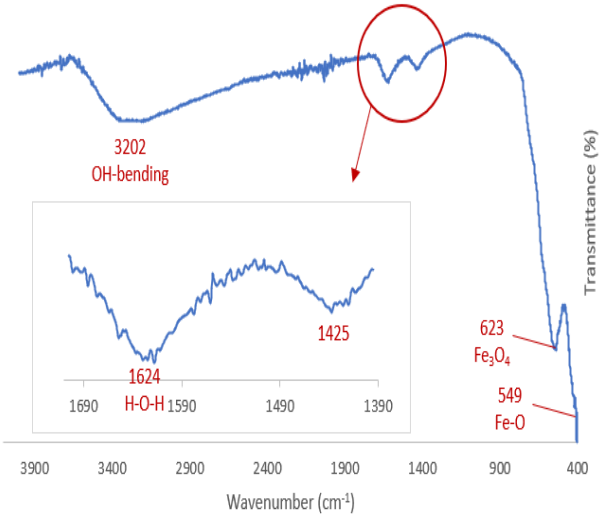

Figure 3. FTIR spectra of naked Fe_3O_4

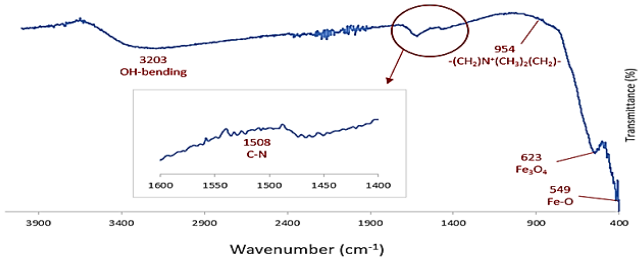

Figure 4. FTIR spectra of PDDA-Fe_3O_4 NPs

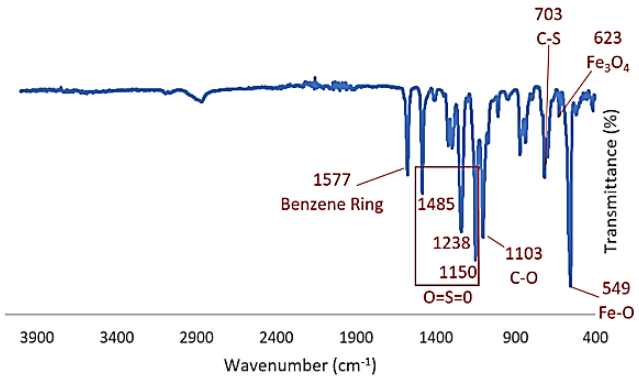

Figure 5. FTIR spectra of PDDA-Fe_3O_4@PES microcapsule

According to [11], the wide characteristic bands centering at around 3200 cm^{-1} were caused by the existence of adsorbed or free water molecules that were attributed to the hydroxyl group's OH-bending, as could be observed in Figure 3. Meanwhile, the wavelength of 549 cm^{-1} was assigned to the Fe-O vibration within the Fe_3O_4 crystalline lattice [12]. Besides, the symmetry degeneration occurring on octahedral B sites was associated with the following splitting peak at 623 cm^{-1} [13]. This demonstrated that the co-precipitation approach was effective in producing Fe_3O_4 NPs. Next, according to [14], peak at 1508 cm^{-1} was attributed to the C-N stretch while peak at 954 cm^{-1} was the $-(CH_2)N+(CH_3)_2(CH_2)-$ vibration in aliphatic PDDA. Both peaks have demonstrated the effective functionalisation of PDDA polymer on Fe_3O_4 NPs (Figure 4). Besides, based on Figure 5, the existence of PES polymer was demonstrated by the strong absorption peaks of the C-O bond stretching, sulfonyl group (1458 cm^{-1}, 1238 cm^{-1}, and 1150 cm^{-1}) and benzene ring (1577 cm^{-1}) [15].

3.2. Fit Statistics and ANOVA Results by Design Expert

3.2.1. Statistical Analysis of Results

Table 2 shows the removal of MB by PDDA-Fe_3O_4@PES microcapsule in various combinations of process parameters. The removal of MB varied from 1.5% to 93.20% across different combinations of process parameters. Experimental data obtained from the DOE were subjected to multiple regression analysis to establish a suitable polynomial model describing the results. Based on the F-value and probability value, the software recommended a quadratic model for both the adsorption and degradation of MB, as illustrated in Table 3. Quadratic model with the smallest standard deviation and largest coefficient of determination (R_2) values could adequately describe the process. From the R_2 value that relates the experimental and predicted response developed by the model, it was clear that the analysed process parameters could sufficiently explain the percentage of MB removal variability up to 98.90 %. In other words, the model could not explain only 1.1 % of the variation. Also, the adjusted R_2 value was in close agreement with the predicted R_2 value with the difference of less than 0.2. This implied that the responses were well described by the quadratic regression model.

Table 2. Removal of MB at various combinations of process parameters

Run	Microsphere Dosage (g/L)	Initial MB Conc. (mg/L)	Solution pH	**Contact Time (min)**	**H2O2 Concentration (mol/L)**	**Removal of MB (%)**
1	24	22	4	112	0.74	12.31
2	16	22	4	112	0.74	4.42
3	30	30	6	150	0.55	76.13
4	16	22	8	188	0.36	87.78
5	20	30	6	150	0.55	77.04
6	16	22	4	188	0.36	4.02
7	24	38	4	188	0.74	17.31
8	20	10	6	150	0.55	64.73
9	20	30	6	60	0.55	37.49

10	24	22	8	188	0.36	86.99
11	10	30	6	150	0.55	42.53
12	20	30	6	150	0.55	80.09
13	20	30	6	150	0.55	78.35
14	20	50	6	150	0.55	42.35
15	16	38	8	188	0.36	86.93
16	16	22	8	188	0.74	88.88
17	20	30	6	150	0.55	80.02
18	16	22	8	112	0.74	83.63
19	24	38	8	188	0.36	81.55
20	20	30	6	150	0.55	76.2
21	24	38	8	112	0.74	81.18
22	24	22	4	112	0.36	10.78
23	16	22	4	112	0.36	3.34
24	24	38	4	112	0.36	7.53
25	20	30	2	150	0.55	1.50
26	24	22	4	188	0.36	18.05
27	16	38	8	112	0.74	85.12
28	20	30	6	150	0.55	78.33
29	24	22	4	188	0.74	22.31
30	16	38	4	188	0.36	5.61
31	16	38	8	112	0.36	81.26
32	24	38	8	112	0.36	81.51
33	24	38	8	188	0.74	84.18
34	24	38	4	112	0.74	14.23
35	16	38	4	112	0.74	9.08
36	16	38	8	188	0.74	89.83
37	20	30	6	150	0.55	78.37
38	16	22	4	188	0.74	6.42
39	24	38	4	188	0.36	9.22
40	20	30	6	150	0.55	81.31
41	20	30	6	240	0.55	75.74
42	16	38	4	112	0.36	3.78
43	24	22	8	112	0.74	87.37
44	20	30	6	150	0.10	8.67
45	16	38	4	188	0.74	12.88
46	20	30	10	150	0.55	93.2
47	20	30	6	150	1.00	43
48	24	22	8	188	0.74	89.73
49	16	22	8	112	0.36	82.45
50	24	22	8	112	0.36	82.66

Table 3. Model summary statistics for removal of MB

Source	Std Dev.	R_2	Adjusted R_2	Predicted R_2	Comment
Linear	1.13	0.8866	0.8737	0.8604	
2FI	1.09	0.9185	0.8825	0.8766	
Quadratic	0.4328	0.9890	0.9813	0.9608	Suggested
Cubic	0.3242	0.9970	0.9895	0.9189	Aliased

Table 4. ANOVA results for quadratic model on the removal of MB

Source	Sum of Squares	df	Mean Square	F-value	p-value
Model	486.49	20	24.32	129.87	< 0.0001
A	6.42	1	6.42	34.26	< 0.0001
B	0.6397	1	0.6397	3.42	0.0748
C	412.47	1	412.47	2202.20	< 0.0001
D	7.55	1	7.55	40.30	< 0.0001
E	9.05	1	9.05	48.31	< 0.0001
AB	2.55	1	2.55	13.60	0.0009

AC	9.85	1	9.85	52.58	0.0002
AD	0.5882	1	0.5882	3.14	0.0869
AE	0.4979	1	0.4979	2.66	0.1138
BC	1.07	1	1.07	5.69	0.0238
BD	0.0199	1	0.0199	0.1065	0.7465
BE	0.3766	1	0.3766	2.01	0.1669
CD	0.1202	1	0.1202	0.6419	0.4295
CE	0.5908	1	0.5908	3.15	0.0862
DE	0.0485	1	0.0485	0.2587	0.6148
A^2	2.60	1	2.60	13.90	0.0008
B^2	4.51	1	4.51	24.10	< 0.0001
C^2	16.71	1	16.71	89.20	< 0.0001
D^2	3.21	1	3.21	17.16	0.0003
E^2	20.26	1	20.26	108.14	< 0.0001
Lack of Fit	4.22	23	0.1835	0.9097	0.53

3.2.2. Development of Regression Model Equation

According to the suggested quadratic model, the empirical relation between the responses and independent parameters in term of coded factors are represented by the second-order polynomial equation as shown in Equation 2.

$$Removal\ of\ MB\ (\%) = 1.89 + 0.3849\ A + 3.09\ C + 0.4175\ D + 0.4571\ E - 0.2850\ B^2 - 0.5483\ C^2 - 0.6037\ E^2 \quad (2)$$

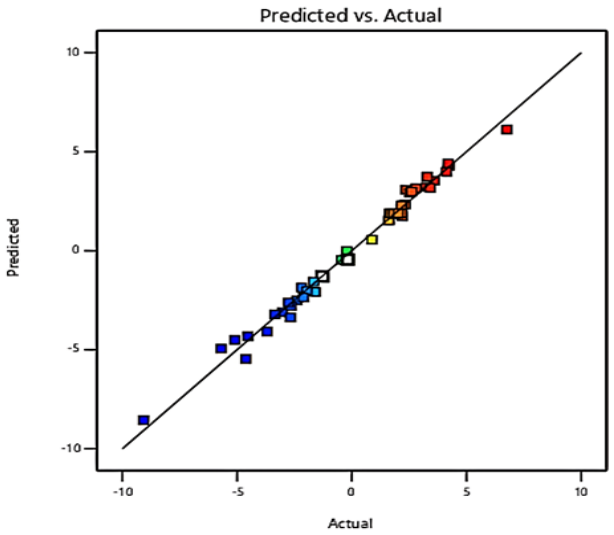

Figure 6. Graph of predicted values versus actual values on removal of MB

Figure 6 shows the predicted versus actual results on the removal of MB using the developed quadratic model. As shown in the figure, the experimental values scattered perfectly around the predicted slope with the R_2 value close to unity at 0.9890, indicating that the developed model equation devised successfully encapsulates the relationship between the process parameters and the removal MB using PDDA-Fe_3O_4@PES microcapsule.

3.2.3. ANOVA

ANOVA was employed to analyze the experimental data at 95 % confidence interval to identify the effects of all process parameters on the removal of MB. The ANOVA results for the removal of MB are displayed in Table 4. From the table, Fisher test gives a F-value of 129.87 accordingly to the quadratic model developed for removal MB; showing that the model term is significant. The p-value, being less than 0.05, indicates significance at a 95% confidence interval (CI) for the developed model. Hence, it can be inferred that the quadratic models chosen adequately to represent the actual removal of MB by using PDDA-Fe_3O_4@PES microcapsule.

3.3. Effect of Various Parameters to MB Removal Efficiency

3.3.1. Effect of PDDA-Fe_3O_4@PES Microcapsule Loading to MB Removal Efficiency

The effect of microcapsule loading on the percentage of removal was studied in the range of 10 to 30 g/L with other parameters remained constant. Figure 7 shows the effect of microcapsule loading on the removal efficiency of MB.

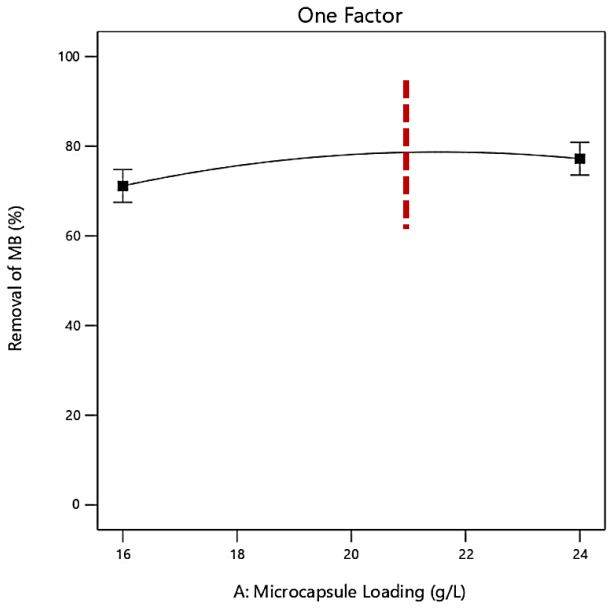

Figure 7. Effect of microcapsule loading on the removal efficiency of MB. Experimental condition: [MB] = 30 ppm; pH = 6; contact time = 150 minutes; [H_2O_2] = 0.55 mol/L

It can be clearly seen that the percentage MB removal increases when the microcapsule loading increases. However, the removal percentage decrease slightly after exceeding the 21 g/L. Increase of microcapsule loading indicated for the increment of microcapsule the number of active sites that are accessible for the removal of MB molecules. The active sites in the PDDA-Fe_3O_4@PES microcapsule can be divided into active sites for adsorption process and active sites for the Fenton-like degradation process. Specifically, the PES shell of the microcapsule act as the active sites for the adsorption process to take place due to the electrostatic force of attraction between cationic MB and the negatively charged PES polymer [7]. Meanwhile the PDDA-Fe_3O_4 NPs embedded in the microcapsule served as the active sites for the Fenton-like degradation process in the presence of H_2O_2 [6]. However, when the microcapsule loading exceeds the 21 g/L the removal of MB dropped slightly. An excess loading of Fe_3O_4 NPs in the system would generate more hydroxyl radical (•OH). Such situation would cause recombination of •OH to occur in which the excess •OH began to react with H2O2 in the valence bond [16]. Eventually, the free •OH for MB degradation became lesser and the removal of MB dropped slightly.

3.3.2. Effect of Initial MB Concentration to MB Removal Efficiency

The effect of initial MB concentration on the percentage of removal was studied in the range of 10 to 50 ppm with other parameters remained constant. Figure 8 shows the effect of initial MB concentration on the removal efficiency of MB.

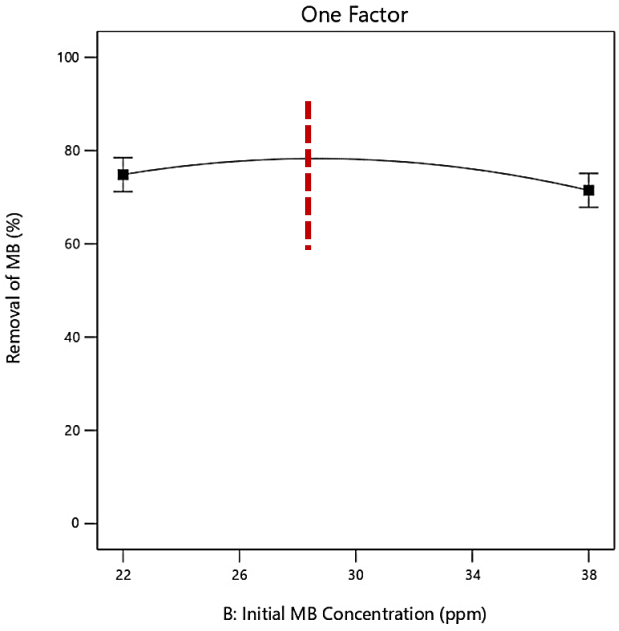

Figure 8. Effect of initial MB concentration on the removal efficiency of MB. Experimental condition: microcapsule loading = 20 g/L; pH= 6; contact time = 150 minutes; [H_2O_2] = 0.55 mol/L

By interpreting the graph, it could be clearly seen that before 28 ppm, the percentage of removal of MB increases when the initial MB concentration increases. However, the removal percentage decreases after exceeding 28 ppm. According to [17], the adsorption rate was generally influenced by the concentration gradient between the adsorbate and the adsorbent. Therefore, higher initial concentration of MB created higher concentration gradient in the system which in turn resulted in a greater driving force for the MB molecules to diffuse from the bulk solution to the surface of PDDA-Fe_3O_4@PES microcapsule.

However, there may be a point at which the adsorption process approached saturation, after which further increase of the concentration gradient may not significantly increase the adsorption rate. This was because there may be a limit to the number of adsorption sites available on the adsorbent surface, and once these sites were occupied, further adsorption may be prohibited. This phenomenon was in agreement with the current study, where the dye removal percentage decreases after the initial MB concentration exceeds the saturation conditions. Similar observation was also reported by [18] in the study of removal of cationic and anionic heavy metals from water by using 1D and 2D-carbon structures decorated with magnetic NPs.

3.3.3. Effect of Solution pH to MB Removal Efficiency

The effect of pH of solution on the removal efficiency was studied in the range of pH 2 to pH 10 with other parameters remained constant. As shown in Table 4, pH was the parameter with the most significant effect to the removal of MB because of having the highest F-value. Figure 9 shows the effect of pH on the removal efficiency of MB.

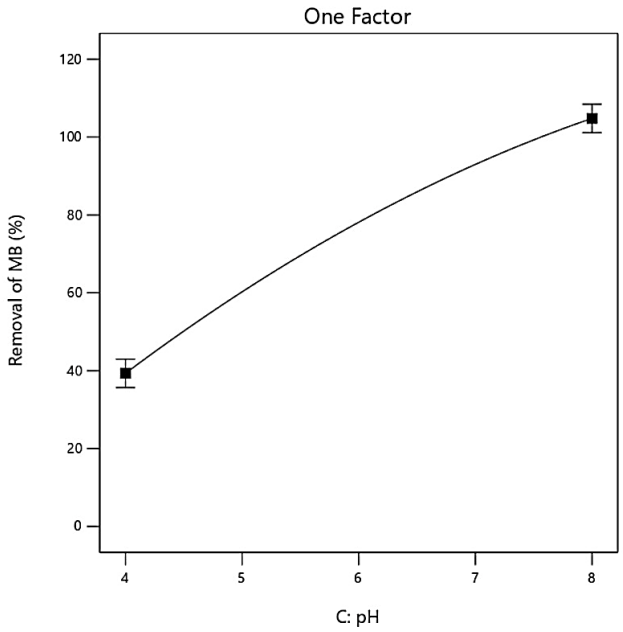

Figure 9. Effect of solution pH on the removal efficiency of MB. Experimental condition: microcapsule loading = 20 g/L; [MB] = 30 ppm; contact time = 150 minutes; [H_2O_2] = 0.55 mol/L

At acidic pH (2.0 – 4.0), the excess hydrogen ions in solution competed the actives sites with MB ions, and eventually contributed to low adsorption capacity of the adsorbent. The microcapsule surface was protonated and saturated with hydronium ions at lower pH, which caused the surface charge to become net positive and repelled the positively charged MB ions. As a result, low adsorption capacity was observed at lower pH [18].

Whereas at higher pH (6.0 – 8.0), a negatively charged microcapsule surface would be obtained. This might be attributed by deprotonation or ionization process in alkaline condition. In general, when the pH of a solution increases, the concentration of hydroxide ions increases as well. These ions would adsorb to the microcapsule surface and cause the microcapsule to become negatively charged [19]. As a result, the positively charged MB ions tend to get attracted towards the negatively charged microcapsule via electrostatic attraction.

3.3.4. Effect of Contact Time to MB Removal Efficiency

The effect of contact time on the percentage of removal was studied in the range of 60 to 240 minutes with other parameters remained constant. Figure 10 shows the effect of contact time on the removal efficiency of MB.

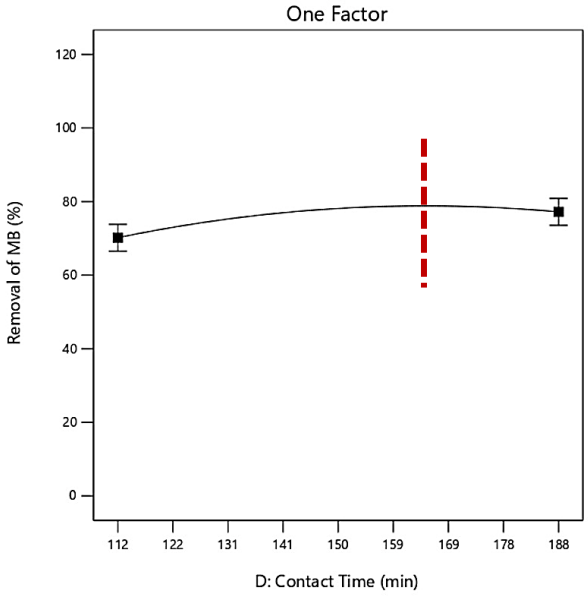

Figure 10. Effect of contact time on the removal efficiency of MB. Experimental condition: microcapsule loading = 20 g/L; [MB] = 30 ppm; pH= 6[H_2O_2] = 0.55 mol/L

From the graph, it can be clearly seen that before reaching saturation point which is approximately 163 min, the percentage of MB removal increased over time. However, the removal percentage decrease slightly after that.

Rapid dye removal could be observed at the beginning of the removal process was because of the high availability of free active sites in the microcapsule. However, when the removal process was prolonged, the number of available active sites decreased, leading to a decrease in the adsorption rate until it reached equilibrium. In addition, bulk phase phenomena (a condition in which the concentration of MB molecules in the interior of the microcapsule was less than the concentration of MB molecules on the microcapsule's surface) would lead to the repletion of MB molecules, prohibiting the MB molecules to diffuse into the microcapsule [20].

3.3.5. Effect of H_2O_2 Concentration to MB Removal Efficiency

The effect of H_2O_2 concentration on the MB removal was studied in the range of 0.1 to 1.0 mol/L with other parameters remained constant. Figure 11 shows the effect of H2O2 concentration on the removal efficiency of MB.

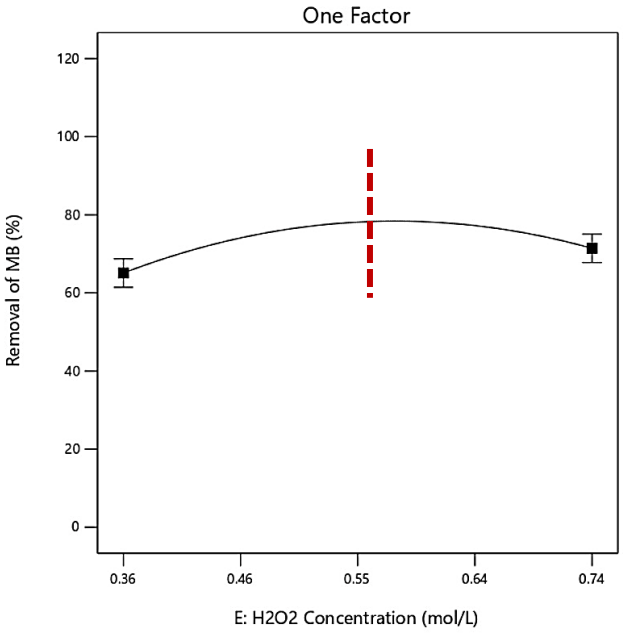

Figure 11. Effect of H_2O_2 on the removal efficiency of MB. Experimental condition: microcapsule loading = 20 g/L; [MB] = 30 ppm; pH= 6; contact time = 150 minutes

The removal of MB increased steadily when the H2O2 concentration increased from 0.36 to 0.58 mol/L. However, the removal percentage decreased after exceeding the H_2O_2 concentration of 0.58 mol/L. H_2O_2 did not involve in the adsorption process but played a significant role in the Fenton-like degradation process in the presence of Fe_3O_4. Higher H_2O_2 concentrations may produce more •OH, which oxidised the MB molecules.

However, as the H_2O_2 concentration increased until the system become excessive with H_2O_2, side reaction occurred between H_2O_2 and •OH to produce •OOH radical and water. This reduces the free •OH for the degradation process. It was reported that the •OOH radical is far less reactive than • OH radical [21].

Furthermore, according to [22], •OOH radical could undergo further reaction with •OH to produce H_2O and O_2. This side reaction (Equation 3) also contributed for the

decrease in MB removal percentage since free •OH that accounted for Fenton-like degradation became lesser.

$$\bullet OOH + \bullet OH \rightarrow H_2O + O_2 \quad (3)$$

Such result trend obtained in this study was in line with those reported in literatures in which greater concentrations of H_2O_2 caused adverse effects on the Fenton-like degradation [23, 24]. This finding seemed beneficial because it allowed for less usage of the corrosive and irritating H_2O_2 but still achieve high MB removal. Additionally, a low H_2O_2 concentration utilized in the MB removal process could also lower the operating costs and reduce corrosion damage to equipment.

3.4. Simultaneous Adsorption and Degradation in MB Removal

Evidence of concurrent adsorption and degradation during MB removal using PDDA-Fe_3O_4@PES microcapsules is apparent when comparing the MB removal efficiencies with corresponding process parameters for runs 5, 44, and 46 as presented in Table 2. The significant enhancement in MB removal from 8.67% to 77.04% when comparing run 44 to run 5, achieved by increasing H_2O_2 concentration from 0.1 mol/L to 0.55 mol/L, indicates the generation of more •OH radicals for MB degradation. Similarly, the further increase in removal to 93.2% when comparing run 5 and 46, with the pH raised from 6 to 10 while other parameters remained constant, underscores the pivotal role of pH in the adsorption process. Hence, it can be inferred that simultaneous adsorption and degradation occurred within the system.

3.5. Optimization Results

Figure 12 displays the limits for each of the process parameters used in the optimization procedure. The software predicted that 94.29 % of MB removal could be successfully achieved by using the PDDA-Fe_3O_4@PES microcapsule at the optimum condition of 21 g/L microcapsule loading, 25 ppm initial MB concentration, pH 7, 127 min contact time and 0.45 mol/L H_2O_2 concentration.

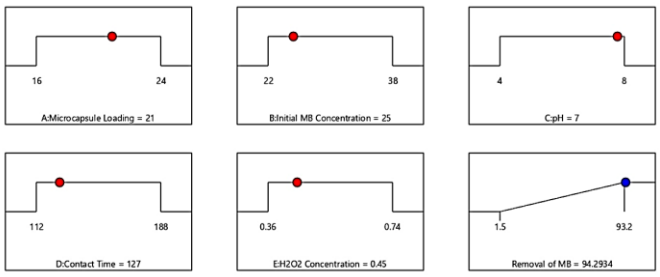

Figure 12. Optimization Results Obtained from Design Expert

The predicted removal percentage of MB obtained from Design Expert was subsequently verified by conducting three repeated experimental runs using the suggested optimum conditions. The percentage error was then calculated by comparing the predicted removal with the experimental removal. The equation used to calculate the percentage error is shown in Equation 4.

$$Percentage\ error\ (\%) = \left| \frac{(MB\ removal_{experimental} - MB\ removal_{predicted})}{MB\ removal_{experimental}} \right| \times 100 \quad (4)$$

As observed in Table 5, the errors between the predicted and experimental removal of MB were less than 5 % indicating that the model is capable in predicting the optimum condition accurately.

Table 5. Verification of optimum conditions for removal of MB using PDDA-Fe_3O_4@PES microcapsule.

Run	Predicted Removal of MB (%)	Experimental Removal of MB (%)	Percentage error (%)
1	94.29	93.01	1.38
2	94.29	92.28	2.18
3	94.29	93.53	0.81
Average		92.94	

The removal of MB from aqueous solutions have been investigated using various materials in recent studies. Activated carbon derived from Ficus carica bast (FCBAC) demonstrated an 85% removal rate of MB [25]. On the other hand, biochemical materials such as silica gel powder (SG), silica gel mixed with eggshell powder (SG-ES), and a mixture of silica gel with sand from the western Iraqi desert (SG-SI) exhibited removal efficiency of 86%, 80% and 57% respectively [26]. Notably, magnetic activated carbon (Fe_3O_4-RAC) achieved an impressive 95.2% removal rate of MB [27]. These findings highlighted the diverse range of materials that can be utilized for effective water purification, each offering unique advantages in the removal of contaminants like MB from water sources. The PDDA-Fe_3O_4@PES microcapsule synthesized in this study demonstrated a competitive removal efficiency of 92.94%, placing it among the top-performing materials. The composite's enhanced performance was attributed to the synergistic effects of Fe_3O_4, PES, and PDDA, which together improve adsorption capacity through electrostatic interactions and provide additional benefits such as magnetic responsiveness and potential catalytic activity in Fenton-like processes. This comparison underscored the strong competitiveness of PDDA-Fe_3O_4@PES among newly developed materials for MB removal, positioning it as a promising candidate for practical wastewater treatment applications.

4. CONCLUSION

In this study, PDDA-Fe_3O_4@PES microcapsule was successfully synthesized by using the phase inversion method. The PDDA-Fe_3O_4@PES microcapsule exhibited adsorptive and catalytic capabilities in the removal of MB which is categorized as cationic pollutant. A high MB removal up to 92.94 % was obtained under the optimum

conditions of 21 g/L microcapsule loading, 25 ppm initial MB concentration, pH 7, 127 min contact time and 0.45 mol/L H2O2 concentration. As a conclusion, the application of the trifunctional PDDA-Fe_3O_4@PES microcapsule in the removal of cationic pollutants is a potential breakthrough technology for water remediation which worth more extensive investigations. Firstly, further research on the reusability of PDDA-Fe_3O_4@PES microcapsules is essential. Additionally, a more detailed investigation into the kinetics and adsorption isotherms will enhance the understanding of the dye removal mechanism of these microcapsules. Such studies will facilitate the design of adsorption systems and predict adsorption performance.

ACKNOWLEDGMENTS

The research was supported by the Ministry of Higher Education (MoHE), Malaysia, through the Fundamental Research Grant Scheme (FRGS/1/2021/TK0/UTAR/02/36) and Universiti Tunku Abdul Rahman Research Fund (UTARRF) under a grant number of IPSR/RMC/UTARRF/2023-C2/G02.

REFERENCES

[1] I. Khan, K. Saeed, I. Zekker, B. Zhang, A. H. Hendi, A. Ahmad, S. Ahmad, N. Zada, H. Ahmad, L. A. Shah, T. Shah and I. Khan, "Review on Methylene Blue: Its Properties, Uses, Toxicity and Photodegradation," *Water*, vol. 14, no. 2, p. 242, 2022.

[2] C. J. Madadrang, H. Y. Kim, G. Gao, N. Wang, J. Zhu, H. Feng, M. Gorring, M.L. Kasner AND S. Hou, "Adsorption Behavior of EDTA-Graphene Oxide for Pb (II) Removal," *ACS Applied Materials & Interfaces*, vol. 4, no. 3, pp. 1186–1193, 2012.

[3] Z. Cai, X. Deng, Q. Wang, J. Lai, H. Xie, Y. Chen, B. Huang and G. Lin, "Core-shell granular activated carbon and its adsorption of trypan blue," *Journal of Cleaner Production*, vol. 242, p. 118496, 2020.

[4] T. Velempini, MEH. Ahamed, and K. Pillay, "Heavy-metal spent adsorbents reuse in catalytic, energy and forensic applications- a new approach in reducing secondary pollution associated with adsorption," *Results in Chemistry*, vol. 5, p. 100901, 2023.

[5] X. Wang, B. Ma, W. Fu, and H. Yang, "Triethylenetetramine promoted rGO-Fe3O4 nanocomposites for highly efficient Fenton-like reaction," *Journal of water process engineering*, vol. 31, pp. 100814–100814, 2019.

[6] L. Hou, L. Wang, S. Royer, and H. Zhang, "Ultrasound-assisted heterogeneous Fenton-like degradation of tetracycline over a magnetite catalyst," *Journal of Hazardous Materials*, vol. 302, pp. 458–467, 2016.

[7] J. Fito, M. Abewaa, A. Mengistu, K. Angassa, A. D. Ambaye, W. Moyo and T. Nkambule, "Adsorption of methylene blue from textile industrial wastewater using activated carbon developed from Rumex abyssinicus plant," *Scientific Reports*, vol. 13, no. 1, p. 5427, 2023.

[8] W. Y. Tan, S. H. Shuit, S. Lim, S. F. Tee, Y. L. Pang, and Q. H. Ng, "Development of high reusability trifunctional polyethersulfones microspheres for the removal of methyl orange," *Journal of Water Process Engineering*, vol. 51, p. 103347, 2023.

[9] S. K. Low, M. C. Tan, and N. L. Chin, "Effect of ultrasound pre-treatment on adsorbent in dye adsorption compared with ultrasound simultaneous adsorption," *Ultrasonics Sonochemistry*, vol. 48, pp. 64–70, 2018.

[10] C. Cheng, A. He, C. Nie, Y. Xia, C. He, L. Ma and C. Zhao, "One-pot cross-linked copolymerization for the construction of robust antifouling and antibacterial composite membranes," *Journal of Materials Chemistry B*, vol. 3, no. 20, pp. 4170–4180, 2015.

[11] F. Ahangaran, A. Hassanzadeh, and S. Nouri, "Surface modification of Fe_3O_4@SiO_2 microsphere by silane coupling agent," *International Nano Letters*, vol. 3, no. 1, 2013.

[12] H. Y. Zhu, X. Song, X. Yang, C. J. Cheng, H. Yu, and H. Zhang, "Smart chiral magnetic nanoparticles for highly efficient enantioseparation of tryptophan enantiomers," *Journal of Materials Science*, vol. 54, no. 4, pp. 2960–2974, 2019.

[13] L. Nalbandian, E. Patrikiadou, V. Zaspalis, A. Patrikidou, E. Hatzidaki, and C. N. Papandreou, "Magnetic Nanoparticles in Medical Diagnostic Applications: Synthesis, Characterization and Proteins Conjugation," *Current Nanoscience*, vol. 12, no. 4, pp. 455–468, 2016.

[14] L. Zhang, D. Yi, and J. Hao, "Poly (diallyldimethylammonium) and polyphosphate polyelectrolyte complexes as an all-in-one flame retardant for polypropylene," *Polymers for Advanced Technologies*, vol. 31, no. 2, pp. 260–272, 2020.

[15] S. Zhu, M. Shi, S. Zhao, Z. Wang, J. Wang, and S. Wang, "Preparation and characterization of a polyethersulfone/polyaniline nanocomposite membrane for ultrafiltration and as a substrate for a gas separation membrane," *RSC Advances*, vol. 5, no. 34, pp. 27211–27223, 2015.

[16] S. A. Abo-Farha, "Photocatalytic Degradation of Monoazo and Diazo Dyes in Wastewater on Nanometer-Sized TiO2," *Journal of American Science*, vol. 6, no. 11, 2010.

[17] R. Jain and S. Sikarwar, "Photocatalytic and adsorption studies on the removal of dye Congo red from wastewater," *International Journal of Environment and Pollution*, vol. 27, no. 1/2/3, p. 158, 2006.

[18] C. Santhosh, R. Nivetha, P. Kollu, V. Srivastava, M. Sillanpää, A. N. Grace and A. Bhatnagar, "Removal of cationic and anionic heavy metals from water by 1D and 2D-carbon structures decorated with magnetic nanoparticles," *Scientific Reports*, vol. 7, no. 1, 2017.

[19] X. Liu, J. Yin, L. Zhu, G. Zhao, and H. Zhang, "Evaluation of a magnetic polysulfone microcapsule containing organic modified montmorillonite as a novel solid-phase extraction sorbent with chlorophenols as

model compounds," *Talanta*, vol. 85, no. 5, pp. 2451–2457, 2011.

[20] T. M. Alslaibi, I. Abustan, M. A. Ahmad, and A. Abu Foul, "Comparative studies on the olive stone activated carbon adsorption of Zn2+, Ni2+, and Cd2+from synthetic wastewater," *Desalination and Water Treatment*, vol. 54, no. 1, pp. 166–177, 2014.

[21] N. Modirshahla, M. A. Behnajady, and F. Ghanbary, "Decolorization and mineralization of C.I. Acid Yellow 23 by Fenton and photo-Fenton processes," *Dyes and Pigments*, vol. 73, no. 3, pp. 305–310, 2007

[22] C. Bouasla, F. Ismail, and M. E.-H. Samar, "Effects of operator parameters, anions and cations on the degradation of AY99 in an aqueous solution using Fenton's reagent. Optimization and kinetics study," *International Journal of Industrial Chemistry*, vol. 3, no. 1, p. 15, 2012.

[23] B. H. X. Che, S. P. Yeap, A. L. Ahmad, and J. Lim, "Layer-by-layer assembly of iron oxide magnetic nanoparticles decorated silica colloid for water remediation," *Chemical Engineering Journal*, vol. 243, pp. 68–78, 2014.

[24] A. Habib, "Decolorization and mineralization of Brilliant Golden Yellow (BGY) by Fenton and photo-Fenton processes," *African Journal of Pure and Applied Chemistry*, vol. 6, no. 14, pp. 153–158, 2012.

[25] D. Pathania, S. Sharma, and P. Singh, "Removal of methylene blue by adsorption onto activated carbon developed from Ficus carica bast," *Arabian Journal of Chemistry*, vol. 10, pp. S1445–S1451, 2017.

[26] T. Juzsakova, A. D. Salman, T. A. Abdullah, R. T. Rasheed, B. Zairka, R. R. Al-Shaikhly, B. Sluser and I. Cretescu, "Removal of Methylene Blue from Aqueous Solution by Mixture of Reused Silica Gel Desiccant and Natural Sand or Eggshell Waste," *Materials*, vol. 16, no. 4, p. 1618, 2023.

[27] Dhilleswara Rao Vaddi, R. Malla, and satyanarayana Geddapu, "Magnetic activated carbon: A promising approach for the removal of methylene blue from wastewater," *Desalination and water treatment*, vol. 317, pp. 100146–100146, 2024.